Early View

Original research article

The methyl-CpG-binding domain 2 facilitates pulmonary fibrosis by orchestrating fibroblast to myofibroblast differentiation

Yi Wang, Lei Zhang, Teng Huang, Guo-Rao Wu, Qing Zhou, Fa-Xi Wang, Long-Min Chen, Fei Sun, Yongman Lv, Fei Xiong, Shu Zhang, Qilin Yu, Ping Yang, Weikuan Gu, Yongjian Xu, Jianping Zhao, Huilan Zhang, Weining Xiong, Cong-Yi Wang

The methyl-CpG-binding domain 2 facilitates pulmonary fibrosis by orchestrating fibroblast to myofibroblast differentiation

Yi Wang[1,#], Lei Zhang[1,#], Teng Huang[1], Guo-Rao Wu[1], Qing Zhou[1], Fa-Xi Wang[1], Long-Min Chen[1], Fei Sun[1], Yongman Lv[2], Fei Xiong[1], Shu Zhang[1], Qilin Yu[1], Ping Yang[1], Weikuan Gu[3], Yongjian Xu[1], Jianping Zhao[1, *], Huilan Zhang[1, *], Weining Xiong[1, 4,*], Cong-Yi Wang[1,*]

[1]The Center for Biomedical Research, Department of Respiratory and Critical Care Medicine, National Health Center (NHC) Key Laboratory of Respiratory Diseases, Tongji Hospital, Tongji Medical College, Huazhong University of Sciences and Technology, 1095 Jiefang Ave, Wuhan 430030, China.

[2]Health Management Center, Tongji Hospital, Tongji Medical College, Huazhong University of Science and Technology.

[3]Department of Orthopedic Surgery and BME-Campbell Clinic, University of Tennessee Health Science Center, Memphis, Tennessee, 38163, USA.

[4]Department of Respiratory and Critical Care Medicine, Shanghai Key Laboratory of Tissue Engineering, Shanghai Ninth People's Hospital, Shanghai Jiaotong University School of Medicine, 639 Zhizaoju Lu, Shanghai, 200011, China.

[#]These authors contributed equally to this work.

*Correspondence should be addressed to: Dr. Cong-Yi Wang (Tel: 86-27-6937-8458; email: wangcy@tjh.tjmu.edu.cn), the Center for Biomedical Research, Tongji Hospital Research Building, Tongji Hospital, Tongji Medical College, Huazhong University of Science and Technology, Wuhan, China; or Dr. Weining Xiong (Tel: 86-21-53316086; E-mail: xiongdoctor@qq.com), Department of Respiratory and Critical Care Medicine, Shanghai Key Laboratory of Tissue Engineering, Shanghai Ninth People's Hospital, Shanghai Jiaotong University School of Medicine; or Drs. Huilan Zhang (Tel: 86-27-8366-5522; email: huilanz_76@163.com) and Jianping Zhao (Tel: 86-27-8366-5521,

email: zhaojp88@126.com), Department of Respiratory and Critical Care Medicine, Tongji Hospital, Tongji Medical College, Huazhong University of Science and Technology, Wuhan, China.

Take home message: MBD2 is upregulated in the myofibroblasts from IPF patients and facilitates the transition of myofibroblast from fibroblast via TβRI/Smad3/Mbd2/Erdr1 positive feedback regulatory loop.

ABSTRACT

Although DNA methylation has been recognized in the pathogenesis of idiopathic pulmonary fibrosis (IPF), the exact mechanisms, however, are yet to be fully addressed. Herein, we demonstrated that lungs originated from IPF patients and mice after bleomycin (BLM)-induced pulmonary fibrosis are characterized by the altered DNA methylation along with overexpression of methyl-CpG-binding domain 2 (MBD2) in myofibroblasts, a reader responsible for interpreting DNA methylome-encoded information. Specifically, depletion of *Mbd2* in fibroblasts or myofibroblasts protected mice from BLM-induced pulmonary fibrosis coupled with a significant reduction of fibroblast differentiation. Mechanistically, TGF-β1 induced a positive feedback regulatory loop between transforming growth factor-β receptor I (TβRI), Smad3 and Mbd2, and erythroid differentiation regulator 1 (Erdr1). TGF-β1 induced fibroblasts to undergo a global DNA hypermethylation along with Mbd2 overexpression in a TβRI/Smad3 dependent manner, and Mbd2 selectively bound to the methylated CpG DNA within the *Erdr1* promoter to repress its expression, through which it enhances TGF-β/Smads signaling to promote fibroblast differentiating into myofibroblast and exacerbate pulmonary fibrosis. Therefore, enhancing Erdr1 expression strikingly reversed established pulmonary fibrosis. Collectively, our data support that strategies aimed at silencing Mbd2 or increasing Erdr1 could be viable therapeutic approaches for prevention and treatment of pulmonary fibrosis in clinical settings.

KEYWORDS: MBD2, Idiopathic pulmonary fibrosis, Erdr1, Fibroblasts, Myofibroblasts

INTRODUCTION

Idiopathic pulmonary fibrosis (IPF) is a prototype of chronic, progressive, and fibrotic lung disease, usually leading to death within 3–5 years following diagnosis [1]. Despite past extensive studies, the pathoetiology underlying IPF, however, remains poorly understood, which rendered its treatment largely unsuccessful [2, 3]. In general, IPF is characterized by the epithelial injury and differentiation of invasive fibroblasts [4]. The differentiation of fibroblast into myofibroblast plays a critical role in fibrotic processes and contributes to the histological features of IPF lung tissues [5, 6]. Upon the stimulation of fibrotic factors such as transforming growth factor-β (TGF-β) and platelet derived growth factor (PDGF), lung fibroblasts differentiate into myofibroblasts, which then produce copious amount of fibrillary extracellular matrix (ECM) proteins including type I collagen and fibronectin, predisposing to the development of matrix stiffness and pathological matrix deposition in the lung mesenchyme [7, 8].

Previous studies demonstrated that DNA methylation, one of the major epigenetic factors, is involved in the pathogenesis of IPF, but the detailed underlying mechanisms are yet to be fully elucidated [9, 10]. The information encoded by the DNA methylome is generally read by a family of methyl-CpG-binding domain (MBD) proteins (e.g., MBD1, MBD2, MBD4 and MeCP2), which selectively bind to the methylated CpG DNA, thereby inhibiting or increasing the transcription of targeted genes [11-13]. In particular, MBD2 possesses the highest binding capacity to the methylated CpG DNA [14], and therefore, is involved in the pathogenesis of obesity [11], ischemic injury [15], autoimmunity [16, 17], diabetes [18] and tumorigenesis [19]. Interestingly, MBD2 was also found to be highly expressed in the lungs of IPF patients and mice following bleomycin (BLM)-induced pulmonary fibrosis. We thus in the present report generated mouse models with specific *Mbd2* deficiency in fibroblasts or myofibroblasts. It was noted that loss of *Mbd2* in fibroblasts or myofibroblasts significantly protected mice from BLM-induced pulmonary fibrosis along with a marked reduction of myofibroblasts by repressing fibroblast differentiation. Mechanistic studies characterized a

TβRI/Smad3/Mbd2/Erdr1 positive feedback regulatory loop. Specifically, TGF-β1 induces fibroblasts to undergo a global DNA hypermethylation along with Mbd2 over-expression in a TβRI/Smad3-dependent manner; while Mbd2 selectively binds to the highly methylated *Erdr1* promoter to repress its expression, through which it enhances TGF-β/Smads signaling to promote fibroblast differentiating into myofibroblast. Collectively, our data support that altered MBD2 expression in fibroblasts is essential for the progression of pulmonary fibrosis, and therefore, strategies aimed at silencing Mbd2 or increasing Erdr1 could be viable treatments to attenuate fibrotic progression in clinical settings.

MATERIALS AND METHODS

Reagents and antibodies

Antibody against Collagen type I was purchased from EMD Millipore (Schwalbach, Germany), while against Prosurfactant Protein C (pro-SPC), Fibronectin and α-SMA were ordered from Abcam (MA, USA). Antibodies for p-Smad2, p-Smad3, Pi3kp85, p-Pi3kp85, p-Akt, Erk1/2, mTOR, p-mTOR, p-Erk1/2, Jnk, p-Jnk, P38 and p-P38 were originated from Cell Signaling Technology (MA, USA). Antibodies against MBD2 and GAPDH were obtained from Santa Cruz Biotechnology (CA, USA), and Erdr1 antibody was derived from Antibody Research Corporation (MO, USA). Murine recombinant TGF-β1 was obtained from PeproTech (London, United Kingdom), while all other reagents were purchased from Sigma (MO, USA), unless otherwise stated.

Human samples

Resected para-carcinoma lung tissues from non-small cell lung cancer patients (NSCLC, n = 6) and lung explant material from IPF patients (n = 8) were collected in Tongji hospital with informed consent. IPF diagnosis was made according to the European Respiratory Society (ERS)/American Thoracic Society (ATS) consensus diagnostic criteria [20]. Partial lung tissues were chopped for optimal cutting temperature compound (OCT) embedding, which were sliced for immunostaining. The

residual lung tissues were resected into 0.5-1cm^3 and stored in liquid nitrogen for Western blotting or DNA methylation assays. The studies were approved by the Human Assurance Committee of Tongji Hospital (TJ-IRB20210942). Clinical data were provided in Supplementary Table 1.

Bleomycin (BLM) induction of pulmonary fibrosis

The *Mbd2*$^{flox/flox}$ mice in C57BL/6 background were generated using the CRISPR–Cas9 system by the Bioray Laboratories Inc (Shanghai, China). Two *loxP* sequences were inserted in the introns flanking the exon 2 of *Mbd2* as described in Fig. 4A. The *Coll1α2*-Cre^{ERT2} and *Acta2*-Cre^{ERT2} transgenic mice were purchased from the Shanghai Model Organism Center, Inc. (Shanghai, China). The *Coll1α2*-Cre^{ERT2+} or *Acta2*-Cre^{ERT2+} mice were crossed with *Mbd2*$^{flox/flox}$ mice to generate *Coll1α2*-Cre^{ERT2+}*Mbd2*$^{flox/flox}$ or *Acta2*-Cre^{ERT2+}*Mbd2*$^{flox/flox}$ mice, respectively. *Mbd2* deficiency in fibroblasts or myofibroblasts were induced by intraperitoneal injection of tamoxifen (75 mg/kg) in *Coll1α2*-Cre^{ERT2+}*Mbd2*$^{flox/flox}$ or *Acta2*-Cre^{ERT2+}*Mbd2*$^{flox/flox}$ mice at 8-week-old to induce fibroblast specific *Mbd2* deficiency (defined as *Mbd2*-CFKO mice), or myofibroblast specific *Mbd2* deficiency (defined as *Mbd2*-CMKO mice)) for five consecutive days. Littermates (*Coll1α2*-Cre^{ERT2-}*Mbd2*$^{flox/flox}$ or *Acta2*-Cre^{ERT2-}*Mbd2*$^{flox/flox}$ mice) administered with equal dose of tamoxifen were used as controls (defined as *Mbd2*-C). Conventional *Mbd2* knockout mice in C57BL/6 background (defined as *Mbd2*$^{-/-}$ mice),) were kindly provided by Dr. Adrian Bird (Edinburgh University, United Kingdom). Wild-type C57BL/6 mice (defined as WT) were derived from Beijing Huafukang Bioscience Co. Ltd. (Beijing, China).

Mbd2-C, *Mbd2*-CFKO, *Mbd2*-CMKO, *Mbd2*$^{-/-}$ and WT mice were anesthetized with 1% pentobarbital sodium (60 mg/kg), followed by intratracheal injection of 0.5 mg/kg BLM (Nippon Kayaku, Tokyo, Japan) in 40 µl of normal saline with a high pressure atomizing needle (Cat: BJ-PW-M, Bio Jane Trading Limited, Shanghai, China). Mice administered with same volume of normal saline served as controls. *Erdr1* lentiviral particles (1 × 10^7 IFU) were injected into the anesthetized animals intratracheally 10

days after BLM injection. Mice administered with mock lentiviral particles were served as controls. The mice were euthanized on day 21 following BLM challenge to assess pulmonary fibrosis. The four lobes of the right lung (superior lobe, middle lobe, inferior lobe and post-caval lobe) were immediately frozen in liquid nitrogen and stored at −80°C. All mice were housed in an SPF facility at the Tongji Hospital with a 12/12h light/dark cycle. All experimental procedures were approved by the Animal Care and Use Committee at the Tongji Hospital (TJH-201901015).

Histological and immunohistochemical analysis

The left lungs of mice were inflated with 200 ul 4% neutral buffered paraformaldehyde, and sliced from the middle region. The left lung upper region was placed in fresh 4% neutral buffered paraformaldehyde for 24h at room temperature. After paraffin embedding, lung from each mouse was sliced into 5 μm sections (3 sections interval of 200 μm) and subjected to H&E and Masson staining. For one single slide, 5 visual fields were randomly selected under 100× magnification to obtain the mean Ashcroft score by two pathologists in a blinded fashion [21] . The left lung lower region was embedded with OCT and stored at −80°C. For immunostaining, the OCT embedded human and mouse lungs were sliced into 7 μm sections. The frozen sections were next probed with antibodies against α-SMA, Pro-SPC, Mbd2 and Erdr1, followed by staining with Alexa Fluor 594-labeled anti-mouse/rabbit or Alexa Fluor 488-conjugated anti-rabbit/mouse antibodies (Invitrogen, CA, USA), respectively. Images were obtained under a fluorescence microscope (Olympus, Shinjuku, Japan).

Culture and treatment of primary lung fibroblasts

Primary lung fibroblasts were isolated from lungs derived from mice, IPF patients and control subjects as reported [22]. The cells were grown at 37°C and 5% CO_2 in DMEM supplemented with 10% FBS, penicillin/streptomycin. The medium was replaced every 3 days. For fibroblast differentiation, the cells were stimulated with recombinant TGF-β1 (10 ng/ml) at indicated time points.

siRNA transfection

Small interfering RNAs (siRNAs) specific for MBD2 and a corresponding scrambled siRNA were purchased from RiboBio (Guangzhou, China) and then transiently transfected into primary lung fibroblasts using the Lipofectamine 3000 (Invitrogen, Shanghai, China) according as reported [27]. Briefly, primary lung fibroblasts were seeded in 12-well plates 24 h before transfection. siRNA transfection was performed once the cells reached 60% confluence. Transfection efficiency was monitored by RT-PCR or Western blotting after 48 h of transfection. The following two siRNAs were used for MBD2: siRNA1 5'-GCA AGA GCG AUG UCU ACU A-3', and siRNA2 5'-GCG AAA CGA UCC UCU CAA U-3' (ribobio, Guangzhou, China). For *Erdr1* siRNA transfection, *Mbd2$^{-/-}$* lung fibroblasts cultured in DMEM supplemented with 10% FBS were transfected with an *Erdr1* siRNA or control siRNA (ribobio, Guangzhou, China) as above. The transfected cells were next stimulated with murine recombinant TGF-β1 (10 ng/ml) at indicated time points, followed by comparison of myofibroblast conversion.

Western blot analysis

The superior lobe of lung tissues from mice and human subjects and cultured cells were homogenized in RIPA lysis buffer (Beyotime, Shanghai, China) supplemented with proteinase inhibitor cocktail tablets (Roche, Wuhan, China), and the proteins were subjected to Western blotting with indicated primary antibodies as previously reported [23]. Briefly, equal amounts of lysates were separated on 10% SDS-polyacrylamide gel and transferred on to polyvinylidene fluoride (PVDF) membranes. The membranes were blocked with 5% nonfat milk for 1 h at room temperature and then incubated with primary antibodies overnight at 4°C. Next, the membranes were incubated for 1 h at room temperature with an HRP-conjugated secondary antibody (Servicebio, Wuhan, China), prior to the visualization of the bands using the chemiluminescence reagents (Pierce ECL, Thermo Scientific, Ulm, Germany). The blots were recorded with the X-ray film and analyzed using the Image Lab 6.0.1 software (Biorad, Munich, Germany).

Quantitative RT-PCR analysis

Total RNA was isolated from the middle lobe of mouse lung and cultured cells using the TRIzol reagent (Takara, Dalian, China). The RNA quantity and quality were measured using a NanoDrop 2000 spectrophotometer (Thermo Scientific, MA, USA). Complementary DNA synthesis was performed using an M-MLV reverse transcriptase kit (Invitrogen, CA, USA). Quantitative RT-PCR was performed using the SYBR Premix Ex Taq (TaKaRa), and the relative expression of each target gene was normalized by *Actb* expression as previously described [24]. The primers used for each target gene were provided in Supplementary Table 2.

Hydroxyproline assays

The hydroxyproline contents in the inferior lobe of right lung were measured by using a hydroxyproline kit (Nanjing Jiancheng Institute, Nanjing, China) as previously described [25]. Briefly, the fresh lung tissues were weighed and alkaline hydrolyzed for 20 min at 100°C. After adjusting pH to 6.0-6.8, the hydrolysates were refined with 25mg active carbon and centrifuged at 3,500 rpm for 10 min. The supernatants were then undergone a series of chemical reactions, and finally OD values were determined at 550 nm using a microplate reader (ELx800, BioTek Instruments, Inc., Winooski, VT). The hydroxyproline content in the lung tissue was given as µg hydroxyproline per g lung tissue by comparing with the hydroxyproline standard.

RNA deep sequencing (RNA-seq)

RNAs from WT and *Mbd2*$^{-/-}$ lung fibroblasts were extracted using an RNA isolation kit (QIAGEN，Shanghai, China), respectively. RNA quality and integrity were determined using the Nanodrop 1000 Spectrophotometer (Thermo Fisher Scientific, MA, USA) and Agilent Bioanalyser (DNA TECH, CA, USA). RNA-seq libraries were multiplexed and loaded per lane into the Illumina HiSeq flow cell v3. All sequencing protocols were carried out as per the manufacturer's instructions using the Illumina HiSeq 1000 system and HiSeq control software.

Chromatin immunoprecipitation (ChIP) assay

ChIP assays were conducted using a ChIP assay kit (Beyotime Biotechnology, Shanghai, China) as reported [26]. Briefly, 1×10^6 lung fibroblasts were cross-linked with formaldehyde, and chromatin fragmentation was carried out according to the protocol provided. The above prepared diluted soluble chromatin solution was then incubated with an Mbd2 antibody overnight at 4°C with rotation. Normal rabbit IgG was used to determine nonspecific bindings. The above mixtures were next incubated with protein A+G agarose beads, and the protein-DNA complexes were eluted out after washes. The eluted DNA was subjected to ChIP-PCR with indicated primers. The primers used for *Erdr1* in the ChIP assay were: F:5'- GGC TTT TTT AAA CTC GAT CCG -3', R: 5'- GGC AGG ACT ACA ACT CCC AG -3'.

Global DNA methylation assay

Global DNA methylation was determined using a MethylFlashTM Methylated DNA Quantification Kit (Epigentek, NY, USA) according to the manufacturer's instructions. Briefly, the methylated DNA was detected using the capture and detection antibodies to 5-methylcytosine (5-mC) and then quantified colorimetrically by reading absorbance at 450 nm using a microplate reader (ELx800, BioTek Instruments, Inc., Winooski, VT).

DNA Bisulfite Sequencing Analysis

Genomic DNA from each preparation was undergone bisulfite conversion using an EZ DNA Methylation-Direct™ Kit (Zymo Research, CA, USA) as previously reported [11, 13]. The resulting products were used as templates to amplify the targeted sequences, and the PCR products were directly cloned into plasmids for sequencing. The methylation state of each targeted sequence was then analyzed by DNA sequencing.

Statistical analysis

Comparisons between groups were undertaken using the Prism software (GraphPad Prism 8.lnk, GraphPad Software Inc). Two experimental groups were compared using the two-tailed Student's t-test (data with normal distribution, homogeneity of variance) or two-tailed Mann–Whitney test (data without normal distribution). Once more than two groups were compared, one-way or two-way analysis of variance with Tukey's multiple comparison test (data with normal distribution) or Kruskal-Wallis test with Dunn's post-hoc tests (data without normal distribution) were used. All experiments were conducted with at least 3 independent replications. The data are presented as the mean ± SEM/SD. In all cases, $p < 0.05$ was considered with statistical significance.

RESULTS

IPF is featured by the altered MBD2 expression and DNA methylation

To address the role of MBD2 and DNA methylation in IPF, we first examined MBD2 expression in the lungs from IPF patients and mice following BLM-induced pulmonary fibrosis. It was noted that IPF patients were featured by the significantly higher expression of α-SMA (a marker of myofibroblasts), and a 7-fold higher MBD2 expression was also noted as compared to the lungs from control subjects (Fig. 1A). Similarly, lungs from mice following BLM induction also exhibited almost a 3-fold higher Mbd2 expression than that of controls, along with overexpression of a-SMA in the fibrotic lungs (Fig. 1B). These results prompted us to characterize the cells showing altered MBD2 expression. We first checked alveolar epithelial type II cell (AECII), as its impairment and apoptosis are one of the major risk factors for IPF initiation [28]. Compared to control subjects, co-immunostaining of MBD2 and prosurfactant protein C (pro-SPC), a marker of AECII, failed to detect MBD2 overexpression in pro-SPC⁺ AECIIs in the lung sections from IPF patients (Supplementary Fig. 1A), and similar results were obtained in lung sections originated from BLM-induced mice (Supplementary Fig. 1B). Consistently, no detectable difference in terms of AECII

apoptosis was observed between BLM challenged WT and *Mbd2*^{-/-} mice (Supplementary Fig. 1C), which was further confirmed by the comparable expression of proapoptotic protein Bax (Supplementary Fig. 1D). We then embarked on mesenchymal cells, which are a major contributor to the progression of matrix deposition and tissue distortion during the course of IPF development [29]. MBD2 was noted to be highly expressed in the lung mesenchymal cells from IPF patients, as evidenced by the co-immunostaining of PDGFR-β (Fig. 1C). Similarly, Mbd2 was almost undetectable in the lung sections originated from control mice, while lung sections derived from fibrotic mice were characterized by the accumulation of mesenchymal cells along with Mbd2 overexpression (Fig. 1D). Given that α-SMA$^+$ and PDGFRα$^+$ mesenchymal cells represent two separate lineages with distinct gene expression profiles in adult lungs [30], we next checked the expression pattern of MBD2 in mesenchymal cells. Indeed, increased number of α-SMA$^+$MBD2$^+$ and PDGFRα$^+$MBD2$^+$ cells were detected in the lung sections from IPF patients and pulmonary fibrotic mice (Fig. 1E and F, Supplementary Fig. 2A and B). However, much more α-SMA$^+$MBD2$^+$ cells but less PDGFRα$^+$MBD2$^+$ cells were observed in the lung sections derived from IPF patients and pulmonary fibrotic mice . To further confirm this observation, we induced WT primary lung fibroblast differentiation with TGF-β1, and noted that the differentiated myofibroblasts were featured by the overexpression of Mbd2 (Fig. 1G).

As aforementioned, MBD2 acts as a reader to interpret DNA methylome-encoded information, the above results rendered us to compare the global DNA methylation levels in the lungs between IPF patients and control subjects as well as in fibrotic lungs from mice following BLM induction. Indeed, a significant global DNA demethylation was noted in the lungs from IPF patients (Fig. 1H), and similar results were also obtained in the fibrotic lungs from mice (Fig. 1I). Collectively, these data support that pulmonary fibrosis is featured by the induction of MBD2 overexpression along with a reduction of global DNA methylation levels.

Mbd2 overexpression depends on TβRI-Smad3 signaling

Next, we conducted Western blot and RT-PCR analysis in primary mouse lung fibroblasts following TGF-β1 stimulation, and demonstrated that TGF-β1 induces Mbd2 overexpression in a dose-dependent manner (Fig. 2A and B). Since canonical TGF-β signaling is crucial for the function of TGF-β1 [31], we thus performed co-immunostaining of Mbd2 and p-Smad2/3 in the above cells following 1 h of TGF-β1 stimulation. As expected, Mbd2 was co-localized with p-Smad2 and p-Smad3 in the differentiated myofibroblasts (Fig. 2C). These findings allowed us to assume that Mbd2 may exert its function downstream to TGF-β1–induced fibrotic signaling. To address this notion, primary mouse lung fibroblasts were treated with SB431542, a selective inhibitor of TGF-β receptor I (TβRI), and SIS3-HCl, a specific inhibitor of Smad3, followed by TGF-β1 stimulation, respectively. TGF-β1 strongly induced fibroblast differentiation as evidenced by the expression of myofibroblast markers fibronectin and α-SMA, whereas inhibition of TβRI by SB431542 (10 nM) (Fig. 2D-E) or Smad3 by SIS3-HCl (5 nM) (Fig. 2F-G) prevented upregulation of fibronectin and α-SMA. More importantly, addition of either SB431542 (Fig. 2D-E) or SIS3-HCl (Fig. 2F-G) completely abolished TGF-β1–induced Mbd2 expression, supporting that Mbd2 overexpression was controlled by the canonical TGF-β signaling, in which TβRI and Smad3 were essential mediators.

Mbd2 is required for fibroblast differentiating into myofibroblast

To assess the functional relevance of Mbd2 overexpression in fibroblasts, we checked the impact of *Mbd2* deficiency on fibroblast differentiation. Remarkably, *Mbd2* deficiency significantly repressed fibroblast differentiation as evidenced by the attenuated expression of fibronectin, collagen I and α-SMA following TGF-β1 stimulation (Fig. 3A). RT-PCR analysis of *Fn1* (Fig. 3B), *Col1a1* (Fig. 3C) and *Acta2* (Fig. 3D) further confirmed this observation. In line with these results, TGF-β1 time-dependently induced Mbd2 expression, and the highest expression was noted

following 48 h of stimulation (Fig. 3E). In addition, *Mbd2* overexpression was highly correlated with fibroblast differentiation, as evidenced by the detection of a positive correlation with *Fn1* ($R^2 = 0.4832$, $p < 0.005$, Fig. 3F), *Col1a1* ($R^2 = 0.7755$, $p < 00001$, Fig. 3G) and *Acta2* expression ($R^2 = 0.9097$, $p < 0.0001$, Fig. 3H). More importantly, inhibition of MBD2 expression by siRNA in the lung fibroblasts derived from IPF patients and Control subjects significantly attenuated the expression of fibronectin, collagen I and α-SMA (Fig. 3I and Supplementary Fig. 3). Collectively, our data suggest that the induction of Mbd2 overexpression is essential for fibroblast differentiation. In support of this notion, *Mbd2* deficiency did not show a significant impact on fibroblast migration (Supplementary Fig. 4A), proliferation (Supplementary Fig. 4B) and apoptosis (Supplementary Fig. 4C), as determined by the Transwell Assay, Edu staining and Annexin V/PI staining, respectively. Together, those data indicate that Mbd2 might selectively modulate fibroblast to myofibroblast differentiation.

Mbd2 deficiency in fibroblasts or myofibroblasts protect mice against BLM-induced lung injury and fibrosis

Since Mbd2 is required for myofibroblast polarization, the next key question is whether *Mbd2* deficiency in myofibroblasts would protect mice against pulmonary fibrosis. We, therefore, generated *Coll1α2*-Cre^{ERT2+}Mbd2$^{flox/flox}$ mice as described, and *Mbd2* deficiency in fibroblasts (*Mbd2*-CFKO) was induced by intraperitoneal injection of tamoxifen for 5 consecutive days (Fig. 4A) on day 12 before BLM induction. *Mbd2* deficiency in collagen I$^+$ cells were confirmed by co-immunostaining of lung sections (Fig. 4B, indicated by white arrows), and was validated by genotyping to detect the null allele (Supplementary Fig. 5A, indicated by a box) and *Coll1α2*-Cre allele in DNA isolated from lung tissues (Supplementary Fig. 5B).

The above mice were sacrificed on day 21 following BLM induction. As compared to the control (*Mbd2*-C) mice, the *Mbd2*-CFKO mice displayed significantly attenuated lung injury and fibrosis as manifested by the H&E and Masson's trichrome staining (Fig.

4C, left panel) along with much lower Ashcroft scores for the severity of pulmonary fibrosis (Fig. 4C, right panel). Consistently, significantly lower levels of hydroxyproline, a major component of fibrillar collagen of all types, were also detected in the *Mbd2*-CFKO mice (Fig. 4D). Western blot analysis of myofibroblast markers fibronectin, collagen I and α-SMA in the lung lysates also indicated significantly lower levels of expression in the *Mbd2*-CFKO mice (Fig. 4E), which were validated by RT-PCR analysis as well (Fig. 4F-H).

To further confirm the critical role of Mbd2 in the process of fibroblast differentiation *in vivo*, we further generated a myofibroblast specific *Mbd2* deficiency mouse model by crossing the *Acta2*-Cre^{ERT2+} mice with the *Mbd2*$^{flox/flox}$ mice as above, and *Mbd2* deficiency in myofibroblasts (*Mbd2*-CMKO) was induced by intraperitoneal injection of tamoxifen for 5 consecutive days on day 10 after BLM induction (Fig. 5A). *Mbd2* deficiency in α-SMA$^+$ cells was confirmed by co-immunostaining of lung sections (Fig. 5B, indicated by white arrows) and genotyping (Supplementary Fig. 5C-D). Indeed, the *Mbd2*-CMKO mice exhibited strikingly alleviated lung injury and fibrosis, as evidenced by the pathologic staining and lower Ashcroft scores, compared with *Mbd2*-C mice, following 21 days of BLM injection (Fig. 5C). Additionally, remarkably lower levels of hydroxyproline were observed in the *Mbd2*-CMKO mice (Fig. 5D). Consistently, the expression of fibrotic markers was evidently blunted in *Mbd2*-CMKO mice as detected by Western blotting (Fig. 5E) and RT-PCR analysis (Fig. 5F-H).

To further validate the observed phenotype, the conventional *Mbd2*$^{-/-}$ mice were further employed for induction of pulmonary fibrosis. Similar as the *Mbd2*-CFKO and *Mbd2*-CMKO mice, the *Mbd2*$^{-/-}$ mice were remarkably resistant to BLM-induced lung injury and fibrosis (Supplementary Fig. 6). Taken together, our data support that loss of *Mbd2* in myofibroblasts protects mice against BLM-induced pulmonary fibrosis.

Mbd2 represses Erdr1 expression to promote fibroblast differentiation

To address more detailed mechanisms by which *Mbd2* deficiency attenuates fibroblast to myofibroblast conversion, we embarked on TGF-β downstream signaling molecules using the *Mbd2-/-* fibroblasts along with TGF-β1 stimulation. Our earlier data indicated that TGF-β1 induction of Mbd2 overexpression depends on TβRI-Smad3 signaling (Fig. 2D-G), and indeed, TGF-β1 stimulated a steady increase of p-Smad2/3 expression. However, it was noted that lack of *Mbd2* significantly attenuated TGF-β1 induced p-Smad2/3 expression (Fig. 6A), but *Mbd2* deficiency did not affect MAPK and PI3K signaling as evidenced by the absence of a significant difference in terms of p-P38, p-Jnk, p-Erk1/2, p-P85, p-Akt and p-mTOR expression between TGF-β1 stimulated WT and *Mbd2-/-* fibroblasts (Supplementary Fig. 7A and B). Similarly, *Mbd2* deficiency did not show a perceptible effect on the expression of repressors Smad7 (Fig. 6B), SMAD Specific E3 Ubiquitin Protein Ligase1 (Smurf1, Fig. 6C), and Smurf2 (Fig. 6D), for the TGF-β-Smad2/3 signaling. Collectively, our data suggest a possible positive feedback regulatory loop between TGF-β-Smads signaling and Mbd2 expression in the lung fibroblasts.

RNA deep sequencing was next employed to compare the expression patterns of genes related to fibroblast differentiation in WT and *Mbd2-/-* lung fibroblasts. Representative Mbd2-associated genes changed by more than 2.5-fold were listed in the heat map (Fig. 6E) and volcano plot (Fig. 6F). We found 1,276 mRNAs, 418 lncRNAs and 1 ncRNA were upregulated, while 1,001 mRNAs, 185 lncRNAs and 2 ncRNA were downregulated in WT lung fibroblasts as compared to that of *Mbd2-/-* lung fibroblasts following TGF-β1 treatment. As expected, the results of RNA-seq and RT-PCR both showed that Mbd2 was highly expressed in WT fibroblasts (Fig. 6G). It was noted that Erdr1, a stress-related survival factor known to inhibit synovial fibroblast migration during the progression of rheumatoid arthritis (RA) [32], was included in a cluster of genes whose expression was upregulated in the *Mbd2-/-* fibroblasts (Fig. 6F). RT-PCR analysis confirmed that TGF-β1-induced *Erdr1* expression was increased by

6.5-fold in *Mbd2*^{-/-} lung fibroblasts as compared to that in WT lung fibroblasts (Fig. 6H). Importantly, upon TGF-β1 stimulation WT fibroblasts manifested an 8-fold decrease of *Erdr1* mRNA levels (Fig. 6H). Consistently, a strikingly dropping Erdr1 mRNA expression was observed in lung tissues originated from IPF patients and control subjects (Supplementary Fig. 8).

Given that Mbd2 serves as a reader to interpret the information encoded by DNA methylation [11-13], the above data prompted us to analyze DNA methylation state of genomic DNA and *Erdr1* promoter by global DNA methylation assay and bisulfite DNA sequencing, respectively. Fibroblasts from the lungs of IPF patients manifested higher global genomic DNA hypermethylation than those originated from control subjects (Supplementary Fig. 9). Remarkably, TGF-β1 induced a global genomic DNA hypermethylation in mouse fibroblasts (Fig. 6I), but no perceptible difference in terms of DNA methylation was noted between WT and *Mbd2*^{-/-} fibroblasts (Fig. 6I). However, bioinformatic analysis (the *Laboratory of Molecular Medicine*, http://www.urogene.org/index.html) predicted one CpG island within the *Erdr1* promoter (Fig. 6J). Bisulfite DNA sequencing confirmed that TGF-β1 induced the *Erdr1* promoter to undergo a DNA hypermethylation at regions from -896 bp to -842 bp (transcription starting site as +1), which contains 12 CpG sites, and 6 of which showed significant methylation differences (Fig. 6K). Similarly, the *Erdr1* promoter showed comparable methylation levels between WT and *Mbd2*^{-/-} fibroblasts (Fig. 6K).

The next key question is whether Mbd2 selectively binds to the above hypermethylated CpG DNAs within the *Erdr1* promoter. ChIP assay was next conducted, and analysis of the resulting ChIP-PCR products confirmed that Mbd2 bound to the *Erdr1* promoter in the regions located at -954 bp to -682 bp, which included the hypermethylated CpG DNA (Fig. 6L). Importantly, DNA methylation dependent luciferase reporter assays confirmed that the transcriptional activity of *Erdr1* was higher in the myofibroblasts with mutant plasmid (no CpG DNA at regions from -896 bp to -842 bp) than those with the WT plasmid after TGF-β1 stimulation (Fig. 6M). Collectively, our data support that TGF-

β1 induces Mbd2 overexpression in the lung fibroblasts by enhancing TβRI-Smad3 signaling, and Mbd2 in turn exacerbates TGF-β1 induced Smad2/3 activation; TGF-β1 also induces fibroblasts to undergo a global DNA hypermethylation, particularly for the *Erdr1* promoter, and Mbd2 binds to the methylated CpG DNA to repress Erdr1 expression.

Erdr1 functions as a repressor to inhibit fibroblast differentiation

We next sought to address the functional relevance of Erdr1 expression in fibroblast differentiation. We first conducted immunostaining of BLM-induced lung sections. Remarkably, $Mbd2^{-/-}$ fibroblasts were featured by the significantly higher number of α-SMA$^-$Erdr1$^+$ cells, while WT fibroblasts were characterized by the markedly higher number of α-SMA$^+$Erdr1$^-$ cells (Fig. 7A), suggesting that Erdr1 may suppress fibroblast differentiation. Next, WT lung fibroblasts were first transduced with mock or *Erdr1* lentiviruses followed by TGF-β1 stimulation. RT-PCR confirmed a 6-fold increase of *Erdr1* expression in Erdr1 transduced fibroblasts as compared to that of mock transduced fibroblasts (Fig. 7B). As expected, compared to mock transduced fibroblasts, *Erdr1* transduced fibroblasts were featured by the significantly reduced expression of fibronectin, collagen I and α-SMA during the course of TGF-β1 stimulation (Fig. 7C). Importantly, suppression of *Erdr1* by siRNA in $Mbd2^{-/-}$ fibroblasts (Fig. 7D) restored their capability to differentiate into myofibroblasts following TGF-β1 stimulation (Fig. 7E). To further confirm the above results, we compared the expression of TGF-β downstream signaling molecules between mock and *Erdr1* lentiviral transduced fibroblasts. Before TGF-β1 stimulation, both types of viral-transduced lung fibroblasts only displayed low levels of p-Smad2 and p-Smad3, while transduction of *Erdr1* lentivirus almost completely abolished TGF-β1 induced Smad2 and Smad3 phosphorylation (Fig. 7F). Importantly, knockdown of *Erdr1* by siRNA almost completely abolished the effect of *Mbd2* deficiency on the suppression of fibroblast differentiation (Fig. 7G). It is worthy of note that Erdr1 in turn attenuated Mbd2 expression, as evidenced by the lower Mbd2 expression in *Erdr1* lentivural transduced

fibroblasts (Supplementary Fig. 10). Collectively, our data support that Erdr1 acts as a strong repressor in TGF-β induced fibroblast differentiation.

Erdr1 protects mice against BLM-induced pulmonary fibrosis

Finally, we sought to establish whether ectopic Erdr1 expression would protect mice against BLM-induced pulmonary fibrosis. We first confirmed that transduction of *Erdr1* lentiviruses (1×10^7 IFU) by intratracheal injection resulted in a 1-fold overexpression of *Erdr1* in the lung (Fig. 8A). WT mice were next subjected to induction of pulmonary fibrosis by BLM injection, and mock or *Erdr1* lentiviruses were intratracheally delivered into the lungs at day 10 after BLM induction. Indeed, transduction of *Erdr1* viruses significantly alleviated BLM-induced lung fibrosis as illustrated by the H&E and Masson's trichrome staining (Fig. 8B, left panel) and fibrotic scores (Fig. 8B, right panel). Consistently, *Erdr1* lentiviral transduced mice manifested much lower levels of hydroxyproline in the lung (Fig. 8C) coupled with a significant reduction for the expression of fibronectin, collagen I and α-SMA (Fig.8D). Together, our data indicate that ectopic Erdr1 expression remarkably reversed the established pulmonary fibrosis.

DISCUSSION

IPF is a progressive and lethal fibrosis in the interstitium of lung lack of effective therapies in clinical setting [33]. In the present report, we conducted studies in patients and animals to dissect the impact of MBD2, a reader for the DNA methylome-encoded information, on the development of pulmonary fibrosis. We illustrated that IPF patients and mice following BLM-induced pulmonary fibrosis were featured by the altered MBD2 expression and DNA methylation. Particularly, MBD2 was overexpressed in myofibroblasts within the lungs during the course of fibrotic processes. Therefore, loss of *Mbd2* in fibroblasts or myofibroblasts provided protection for mice against pulmonary fibrosis following BLM injection by blunting the differentiation of fibroblast into myofibroblast. Mechanistic studies characterized a TβRI/Smad3/Mbd2/Erdr1 positive

feedback regulatory loop. Specifically, TGF-β induces Mbd2 overexpression in a TβRI/Smad3-dependent manner, and Mbd2 selectively binds to the regions of *Erdr1* promoter that contain the hypermethylated CpG DNAs to repress its expression, through which Mbd2 enhances TGF-β/Smads signaling to promote fibroblast differentiating into myofibroblast. The polarized myofibroblast then secretes copious amount of fibrillary ECM proteins to cause matrix stiffness and pathological matrix deposition in the lung mesenchyme, predisposing to the development of pulmonary fibrosis (Fig. 8E). These results not only provide novel insights into the understanding of the role of DNA methylation underlying pulmonary fibrosis, but also demonstrate evidence that targeting Mbd2 or Erdr1 could be a viable approach to inhibit fibroblast transition.

Although substantial effort has recently been devoted to dissect the pathoetiology underlying pulmonary fibrosis, the exact molecular mechanisms unfortunately remain poorly understood. This lack of related information has significantly hampered the development of novel and effective therapies against this devastating disorder, which rendered the survival rate of IPF patients less than 5 years after diagnosis. It is noted that the occurrence of methylation within the gene of CpG islands is closely related to fibrosis, including pulmonary fibrosis [34], liver fibrosis [35], renal fibrosis [36], cardiac fibrosis [37] and skin fibrosis [38]. Herein, we demonstrated that lungs originated from IPF patients and mice with onset of pulmonary fibrosis display altered DNA methylation coupled with MBD2 overexpression. These observations are consistent with previous studies, in which an altered DNA methylation profile was noted in the lungs of IPF patients [9, 10]. Moreover, the levels of DNA methylation related proteins, such as DNA methyltransferase 1 (Dnmt1), Dnmt3a, Dnmt3b, MeCP2 and Mbd2 were highly elevated in the lungs of rat pneumoconiosis model, and suppression of DNA methylation by 5-aza-dC, a Dnmt inhibitor, significantly attenuates pulmonary fibrosis [39]. Together, these data support that DNA methylation is implicated in the pathogenesis of pulmonary fibrosis, but the underlying mechanisms are yet to be fully addressed.

The most exciting discovery in this report is that TGF-β1 induced lung fibroblasts to undergo a global DNA hypermethylation along with Mbd2 overexpression. The induced Mbd2 then selectively binds to the methylated CpG DNA within the *Erdr1* promoter without affecting the methylation levels within the *Erdr1* promoter, by which Mbd2 represses Erdr1 expression to promote the differentiation of fibroblast into myofibroblast, thereby predisposing to the development of IPF. Interestingly, Mbd2 did not seem to have a significant impact on fibroblast migration, proliferation and apoptosis. It seems contradictory in terms of global DNA hypomethylation and hypermethylation of the *Erdr1* promoter in the setting of pulmonary fibrosis. In fact, regulatory mechanisms underlying DNA methylation during the progression of pulmonary fibrosis are very complicated. It is seemly that the effects of DNA methylation on pulmonary fibrosis are dependent on the hypomethylation of genes in favor of fibrosis along with the hypermethylation of critical genes against fibrosis in key types of cells (e.g., macrophages and fibroblasts), rather than the global hypomethylation or hypermethylation in DNAs derived from the lungs or cells. For example, Thy-1, a "fibrosis suppressor" gene, has been noted to be regulated by DNA methylation. Specifically, the fibroblast *Thy-1* promoter region undergoes a DNA hypermethylation upon the stimulation of fibrotic factors, which blunts Thy-1 expression and causes persistent differentiation of fibroblasts during the course of pulmonary fibrosis [40].

The critical issue is the strategies to dissect the pathways relevant to Mbd2 regulation of fibroblast differentiation. Previous studies suggested compelling evidence that TGF-β/Smads signaling is a common feature of fibrotic diseases and has been shown contributing to the transition of fibroblast [5, 6, 41]. These observations prompted us to focus on the canonical TGF-β signaling in our case. Indeed, we found that Mbd2 overexpression in fibrotic condition was dependent on the canonical TGF-β signaling and characterized that TβRI and Smad3 act as the essential mediators. Additionally, loss of Mbd2 markedly inhibited TGF-β1 induced Smad2 and Smad3 phosphorylation

as displayed by the significantly lower levels of p-Smad2 and p-Smad3 in *Mbd2*^{-/-} fibroblasts as compared to that of WT fibroblasts. Collectively, those data provided evidence supporting that Mbd2 enhances canonical TGF-β signaling following TGF-β1 induced overexpression in fibroblasts, thereby contributing to the persistent fibroblast differentiation in pulmonary fibrosis.

The last important question is how Mbd2 promotes TGF-β/Smads signaling. RNA deep-seq was then employed to address the underlying mechanisms. Erdr1, a stress-related survival factor, which has been found to attenuate rheumatoid arthritis by inhibition of synovial fibroblast migration [32], was identified with a 6.5-fold increase in *Mbd2*^{-/-} fibroblasts as compared to that of WT fibroblasts. Interestingly, under physiological condition, the *Erdr1* promoter was hypomethylated. In contrast, upon TGF-β1 stimulation, the *Erdr1* promoter in fibroblasts underwent a steady DNA hypermethylation, and Mbd2 selectively bound to the methylated CpG DNA, by which it suppressed Erdr1 expression. Given the fact that Mbd2 itself does not affect DNA methylation rather by interpreting the effect of DNA methylation on the suppression of gene expression [42], and therefore, *Mbd2* deficiency rendered a failure to decipher the information encoded by the change of DNA methylation in the *Erdr1* promoter following TGF-β1 stimulation, although the change of DNA methylation was indeed induced. We further adopted gain and loss of function studies and confirmed that Erdr1 acts as a negative regulator to suppress fibroblast differentiation by inhibiting TGF-β/Smads signaling. In line with these results, intratracheal administration of *Erdr1* lentivirus significantly attenuated BLM-induced pulmonary fibrosis. Since ectopic Erdr1 expression was administrated during the "fibrotic" phase of the model, it was more applicable and reflective to the clinical management of IPF patients.

Our study has some limitations. As no commercial antibodies for human ERDR1 could be obtained at present, we did not detect the protein level of ERDR1 in the lungs from IPF patients and control subjects, despite that we obtained consistent results by RT-

PCR analysis. Although we demonstrated that Mbd2 was upregulated by TGF-β1 in a TβR1/Smad3-dependent manner, but the detailed mechanisms are yet to be fully elucidated. Furthermore, in the current report we did not address how Erdr1 as a highly conserved autocrine factor represses TGF-β/Smads signaling, which would be a major focus for our follow up studies.

In summary, we have demonstrated that lungs originated from IPF patients and mice with onset of pulmonary fibrosis are characterized by the altered DNA methylation along with MBD2 overexpression. Therefore, loss of *Mbd2* in fibroblast or myofibroblast protected the mice from BLM-induced lung fibrosis. Mechanistically, we have identified a positive feedback regulatory loop between TβRI, Smad3, Mbd2 and Erdr1. Specifically, the activation of TβRI/Smad3 signaling induces Mbd2 overexpression, and Mbd2 in turn further enhances TβRI/Smads signaling through repressing the expression of Erdr1. Upon TGF-β1 stimulation, fibroblasts undergo a global DNA hypermethylation along with Mbd2 overexpression. Erdr1 acts as a negative regulator to inhibit fibroblast differentiation into myofibroblast, while CpG DNAs within the *Erdr1* promoter becomes highly methylated following TGF-β1 stimulation, and Mbd2 selectively binds to those methylated CpG DNAs to repress Erdr1 expression, by which Mbd2 promotes fibroblast differentiation to exacerbate pulmonary fibrosis. Given the fact that Mbd2 itself does not involve the changes of DNA methylation and appears to be dispensable under physiological condition, our data support that strategies aimed at silencing Mbd2 or increasing Erdr1 could be a viable therapeutic approach for prevention and treatment of pulmonary fibrosis in clinical settings.

Acknowledgements

Author contributions

Conflict of interest disclosure

The authors declare no competing financial interests.

REFERENCES

1.   Richeldi L, Collard HR, Jones MG. Idiopathic pulmonary fibrosis. *Lancet* 2017: 389: 1941-1952.

2.   Yao Y, Wang Y, Zhang Z, et al. Chop Deficiency Protects Mice Against Bleomycin-induced Pulmonary Fibrosis by Attenuating M2 Macrophage Production. *Molecular therapy : the journal of the American Society of Gene Therapy* 2016: 24: 915-925.

3.   Kolb M, Raghu G, Wells AU, et al. Nintedanib plus Sildenafil in Patients with Idiopathic Pulmonary Fibrosis. *The New England journal of medicine* 2018: 379: 1722-1731.

4.   Sack C, Raghu G. Idiopathic pulmonary fibrosis: unmasking cryptogenic environmental factors. *The European respiratory journal* 2019: 53.

5.   Boutanquoi PM, Burgy O, Beltramo G, et al. TRIM33 prevents pulmonary fibrosis by impairing TGF-beta1 signalling. *The European respiratory journal* 2020: 55.

6.   Louzada RA, Corre R, Ameziane El Hassani R, et al. NADPH oxidase DUOX1 sustains TGF-beta1 signalling and promotes lung fibrosis. *The European respiratory journal* 2021: 57.

7.   Lagares D, Ghassemi-Kakroodi P, Tremblay C, et al. ADAM10-mediated ephrin-B2 shedding promotes myofibroblast activation and organ fibrosis. *Nature medicine* 2017: 23: 1405-1415.

8.   El Agha E, Moiseenko A, Kheirollahi V, et al. Two-Way Conversion between Lipogenic and Myogenic Fibroblastic Phenotypes Marks the Progression and Resolution of Lung Fibrosis. *Cell stem cell* 2017: 20: 261-273 e263.

9.   Sanders YY, Ambalavanan N, Halloran B, et al. Altered DNA methylation profile in idiopathic pulmonary fibrosis. *American journal of respiratory and critical care medicine* 2012: 186: 525-535.

10. Yang IV, Pedersen BS, Rabinovich E, et al. Relationship of DNA methylation and gene expression in idiopathic pulmonary fibrosis. *American journal of respiratory and critical care medicine* 2014: 190: 1263-1272.

11. Cheng J, Song J, He X, et al. Loss of Mbd2 Protects Mice Against High-Fat Diet-Induced Obesity and Insulin Resistance by Regulating the Homeostasis of Energy Storage and Expenditure. *Diabetes* 2016: 65: 3384-3395.

12. Zhou M, Zhou K, Cheng L, et al. MBD2 Ablation Impairs Lymphopoiesis and Impedes Progression and Maintenance of T-ALL. *Cancer research* 2018: 78: 1632-1642.

13. Zhong J, Yu Q, Yang P, et al. MBD2 regulates TH17 differentiation and experimental autoimmune encephalomyelitis by controlling the homeostasis of T-bet/Hlx axis. *Journal of autoimmunity* 2014: 53: 95-104.

14. Wang Y, Zhang L, Wu GR, et al. MBD2 serves as a viable target against pulmonary fibrosis by inhibiting macrophage M2 program. *Science advances* 2021: 7.

15. Ge Y, Zhang R, Feng Y, et al. Mbd2 Mediates Retinal Cell Apoptosis by Targeting the lncRNA Mbd2-AL1/miR-188-3p/Traf3 Axis in Ischemia/Reperfusion Injury. *Molecular therapy Nucleic acids* 2020: 19: 1250-1265.

16. Wang X, Zhao C, Zhang C, et al. Increased HERV-E clone 4-1 expression contributes to DNA hypomethylation and IL-17 release from CD4(+) T cells via miR-302d/MBD2 in systemic lupus erythematosus. *Cell communication and signaling : CCS* 2019: 17: 94.

17. Yue T, Sun F, Wang F, et al. MBD2 acts as a repressor to maintain the homeostasis of the Th1 program in type 1 diabetes by regulating the STAT1-IFN-gamma axis. *Cell death and differentiation* 2021.

18. Karachanak-Yankova S, Dimova R, Nikolova D, et al. Epigenetic alterations in patients with type 2 diabetes mellitus. *Balkan journal of medical genetics : BJMG* 2015: 18: 15-24.

19. Gong W, Ni M, Chen Z, et al. Expression and clinical significance of methyl-CpG binding domain protein 2 in high-grade serous ovarian cancer. *Oncology letters* 2020: 20: 2749-2756.

20. Raghu G, Collard HR, Egan JJ, et al. An official ATS/ERS/JRS/ALAT statement: idiopathic pulmonary fibrosis: evidence-based guidelines for diagnosis and management. *American journal of respiratory and critical care medicine* 2011: 183: 788-824.

21. Ashcroft T, Simpson JM, Timbrell V. Simple method of estimating severity of pulmonary fibrosis on a numerical scale. *Journal of clinical pathology* 1988: 41: 467-470.

22. Wang Q, Yu J, Hu Y, et al. Indirubin alleviates bleomycin-induced pulmonary fibrosis in mice by suppressing fibroblast to myofibroblast differentiation. *Biomedicine & pharmacotherapy = Biomedecine & pharmacotherapie* 2020: 131: 110715.

23. Hu Y, Yu J, Wang Q, et al. Tartrate-Resistant Acid Phosphatase 5/ACP5 Interacts with p53 to Control the Expression of SMAD3 in Lung Adenocarcinoma. *Molecular therapy oncolytics* 2020: 16: 272-288.

24. Wang Q, Liu J, Hu Y, et al. Local administration of liposomal-based Srpx2 gene therapy reverses pulmonary fibrosis by blockading fibroblast-to-myofibroblast transition. *Theranostics* 2021: 11: 7110-7125.

25. Xu M, Wang X, Xu L, et al. Chronic lung inflammation and pulmonary fibrosis after multiple intranasal instillation of PM2 .5 in mice. *Environmental toxicology* 2021: 36: 1434-1446.

26. Wang Y, Zhu J, Zhang L, et al. Role of C/EBP homologous protein and endoplasmic reticulum stress in asthma exacerbation by regulating the IL-4/signal transducer and activator of transcription 6/transcription factor EC/IL-4 receptor alpha positive feedback loop in M2 macrophages. *The Journal of allergy and clinical immunology* 2017: 140: 1550-1561 e1558.

27. Pan T, Zhou Q, Miao K, et al. Suppressing Sart1 to modulate macrophage polarization by siRNA-loaded liposomes: a promising therapeutic strategy for pulmonary fibrosis. *Theranostics* 2021: 11: 1192-1206.

28. Martinez FJ, Collard HR, Pardo A, et al. Idiopathic pulmonary fibrosis. *Nature reviews Disease primers* 2017: 3: 17074.

29. Haak AJ, Kostallari E, Sicard D, et al. Selective YAP/TAZ inhibition in fibroblasts via dopamine receptor D1 agonism reverses fibrosis. *Science translational medicine* 2019: 11.

30. Biasin V, Crnkovic S, Sahu-Osen A, et al. PDGFRalpha and alphaSMA mark two distinct mesenchymal cell populations involved in parenchymal and vascular remodeling in pulmonary fibrosis. *American journal of physiology Lung cellular and molecular physiology* 2020: 318: L684-L697.

31. Sibinska Z, Tian X, Korfei M, et al. Amplified canonical transforming growth factor-beta signalling via heat shock protein 90 in pulmonary fibrosis. *The European respiratory journal* 2017: 49.

32. Kim KE, Kim S, Park S, et al. Therapeutic effect of erythroid differentiation regulator 1 (Erdr1) on collagen-induced arthritis in DBA/1J mouse. *Oncotarget* 2016: 7: 76354-76361.

33. Speca S, Dubuquoy C, Rousseaux C, et al. GED-0507 is a novel potential antifibrotic treatment option for pulmonary fibrosis. *Cellular & molecular immunology* 2020: 17: 1272-1274.

34. Lee JU, Son JH, Shim EY, et al. Global DNA Methylation Pattern of Fibroblasts in Idiopathic Pulmonary Fibrosis. *DNA and cell biology* 2019: 38: 905-914.

35. Wang L, Marek GW, 3rd, Hlady RA, et al. Alpha-1 Antitrypsin Deficiency Liver Disease, Mutational Homogeneity Modulated by Epigenetic Heterogeneity With Links to Obesity. *Hepatology* 2019: 70: 51-66.

36. Gu Y, Chen J, Zhang H, et al. Hydrogen sulfide attenuates renal fibrosis by inducing TET-dependent DNA demethylation on Klotho promoter. *FASEB journal : official publication of the Federation of American Societies for Experimental Biology* 2020: 34: 11474-11487.

37. Xu X, Friehs I, Zhong Hu T, et al. Endocardial fibroelastosis is caused by aberrant endothelial to mesenchymal transition. *Circulation research* 2015: 116: 857-866.

38. Qiu Y, Gao Y, Yu D, et al. Genome-Wide Analysis Reveals Zinc Transporter ZIP9 Regulated by DNA Methylation Promotes Radiation-Induced Skin Fibrosis via the TGF-beta Signaling Pathway. *The Journal of investigative dermatology* 2020: 140: 94-102 e107.

39. Zhang N, Liu K, Wang K, et al. Dust induces lung fibrosis through dysregulated DNA methylation. *Environmental toxicology* 2019: 34: 728-741.

40. Sanders YY, Pardo A, Selman M, et al. Thy-1 promoter hypermethylation: a novel epigenetic pathogenic mechanism in pulmonary fibrosis. *American journal of respiratory cell and molecular biology* 2008: 39: 610-618.

41. Wang P, Luo ML, Song E, et al. Long noncoding RNA lnc-TSI inhibits renal fibrogenesis by negatively regulating the TGF-beta/Smad3 pathway. *Science translational medicine* 2018: 10.

42. Rao X, Zhong J, Zhang S, et al. Loss of methyl-CpG-binding domain protein 2 enhances endothelial angiogenesis and protects mice against hind-limb ischemic injury. *Circulation* 2011: 123: 2964-2974.
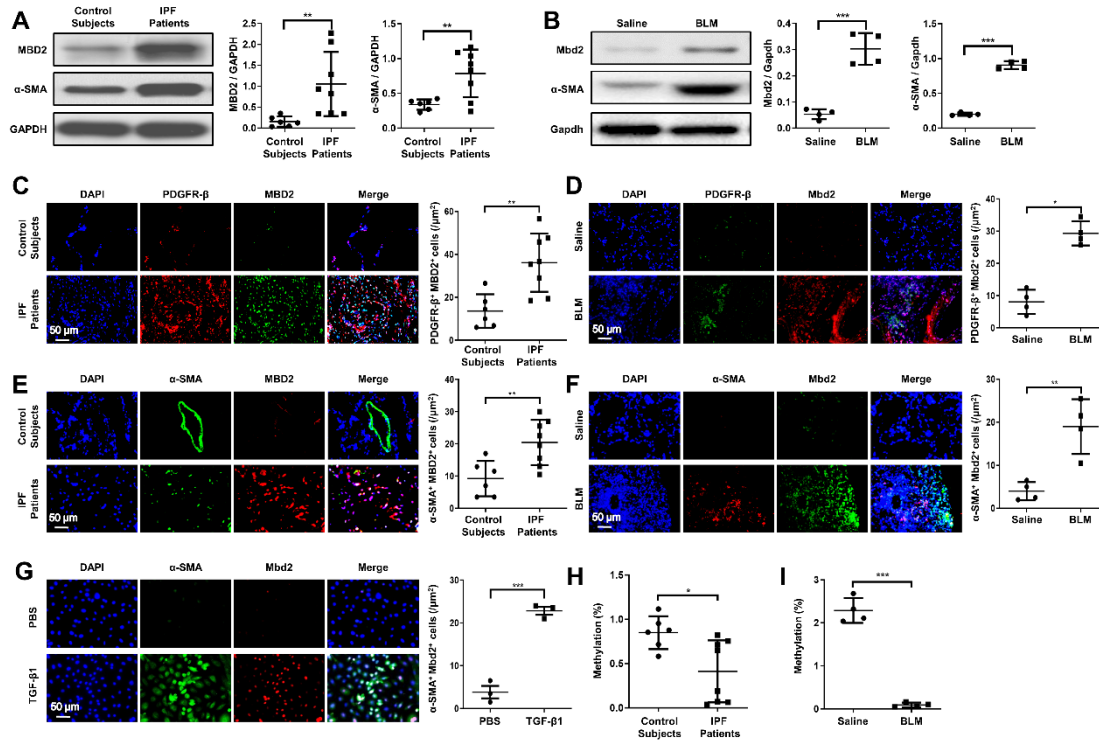
Fig. 1. Analysis of MBD2 expression and DNA methylation in IPF patients and mice with BLM induction. (A) Western blot analysis of MBD2 and α-SMA expression in the lungs of control subjects and IPF patients. **(B)** Western blot analysis of Mbd2 and α-SMA expression in the lungs of mice following 21 days of BLM induction. **(C-D)** Representative results for coimmunostaining of MBD2 and PDGFR-β in the lung sections from patients with control subjects and IPF patients **(C)** and BLM-induced lung sections **(D)**. **(E-G)** Results for coimmunostaining of MBD2 and α-SMA, a myofibroblast marker in the lung sections from patients with IPF and control subjects **(E)**, BLM-induced lung sections **(F)** and TGF-β1-induced fibroblasts **(G).** The nuclei were stained blue by DAPI, and the images were taken under original magnification ×400. **(H)** Global DNA methylation rate in the lungs of control subjects and IPF patients. **(I)** Global DNA methylation rate in the lungs of mice following BLM induction. A total of eight patients with IPF and six control subjects were analyzed. Five mice were analyzed in each group. BLM, Bleomycin; α-SMA, alpha-smooth muscle actin. The data are represented as the mean ± SD. *, $p < 0.05$; **, $p < 0.01$; ***, $p < 0.001$.
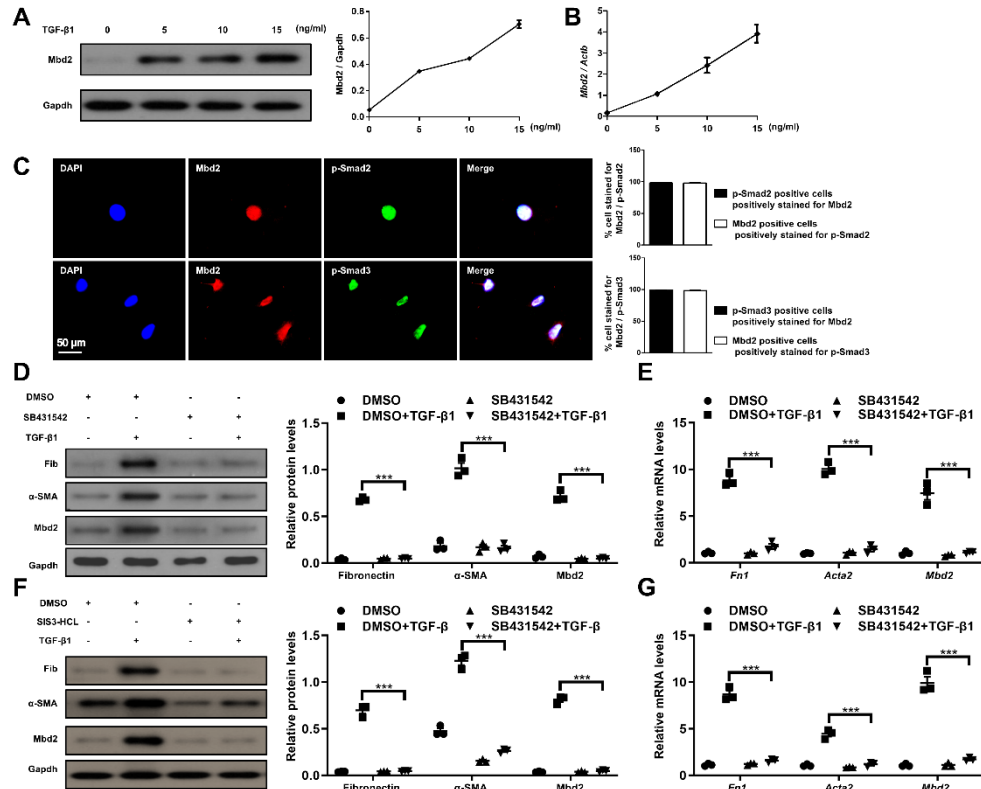
Fig. 2 TGF-β1 induces Mbd2 in a TβRI and Smad3-dependent manner. (A-B) Western blot and RT-PCR analysis of Mbd2 expression in the primary lung fibroblasts following different doses of TGF-β1 induction. **(C)** Results for coimmunostaining of Mbd2 and p-Smad2, Mbd2 and p-Smad3 in the primary lung fibroblasts following TGF-β1 induction for 1h. The nuclei were stained blue by DAPI, and the images were taken under original magnification ×400. **(D-E)** Western blot and RT-PCR analysis of Mbd2 expression in the primary lung fibroblasts pre-treated with SB431542 following TGF-β1 induction. **(F-G)** Western blot and RT-PCR analysis of Mbd2 expression in the primary lung fibroblasts pre-treated with SIS3-HCL following TGF-β1 induction. Fib, Fibronectin; α-SMA, alpha-smooth muscle actin. The data are represented as the mean ± SEM of three independent experiments. ***, $p < 0.001$.
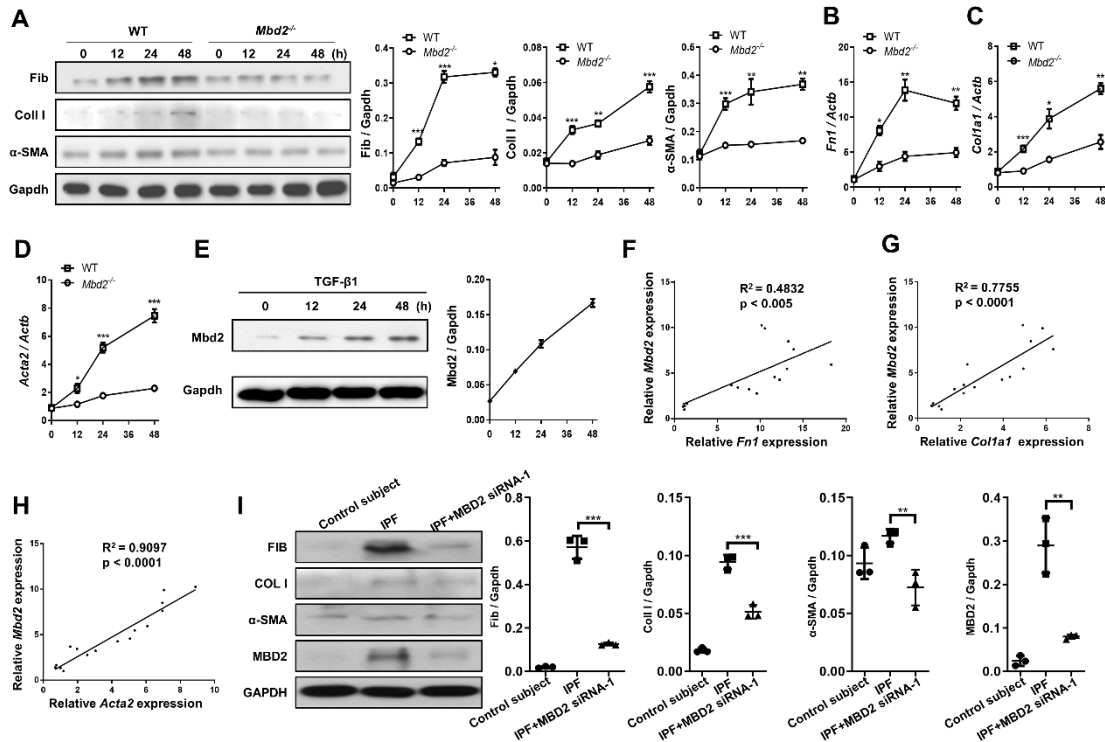
Fig. 3 Loss of *Mbd2* attenuated fibroblast differentiation into myofibroblast. (A) Results for time-course Western blot analysis of fibronectin, collagen I and α-SMA expression in mouse lung fibroblasts following TGF-β1 stimulation. Left panel: A representative Western blot result. Right panel: A bar graph shows the results with three replications. **(B-D)** Results for time-course RT-PCR analysis of *Fn1* **(B)**, *Col1a1* **(C)** and *Acta2* **(D)** in primary mouse lung fibroblasts following TGF-β1 treatment. **(E)** Results for time-course Western blot analysis of Mbd2 expression in mouse lung fibroblasts following TGF-β1 stimulation. **(F-H)** RT-PCR analysis of the correlation between *Mbd2* and *Fn1* **(F)**, *Col1a1* **(G)** and *Acta2* **(H)** expression after TGF-β1 induction. **(I)** Western blot analysis of the expression of fibronectin, collagen I, α-SMA and MBD2 in control subject and IPF patient's lung derived fibroblasts. Fib, Fibronectin; Col I, collagen I; α-SMA, alpha-smooth muscle actin. The data are represented as the mean ± SEM of three independent experiments. *, $p < 0.05$; **, $p < 0.01$; ***, $p < 0.001$.
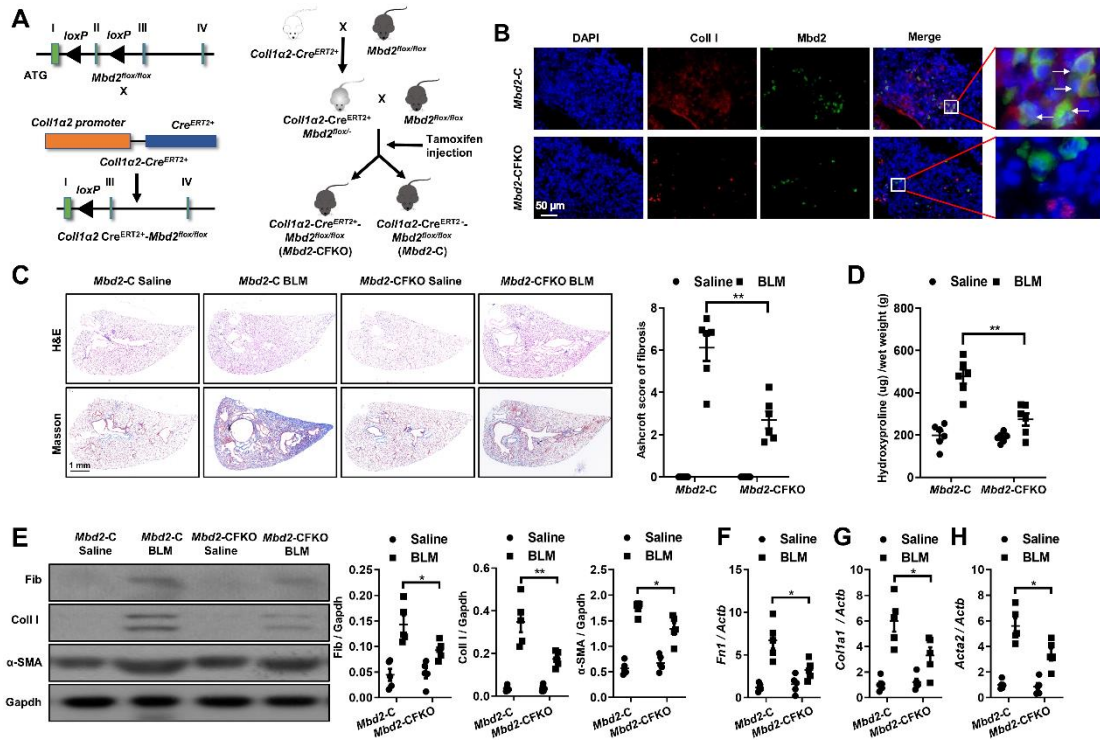
Fig. 4 Comparison of the severity of lung fibrosis between *Mbd2*-CFKO and *Mbd2*-C mice after BLM induction. (A) *Mbd2^flox/flox^* mice were generated by inserting two *loxP* sequences in the same direction into the introns flanked with the exon 2 of MBD2 based on the CRISPR–Cas9 system, which could produce a nonfunctional Mbd2 protein by generating a stop codon in exon 3 after Cre-mediated gene deletion. *Mbd2^flox/flox^* then crossed with the *Coll1α2*-Cre^ERT+^ transgenic mice to get the fibroblast-specific *Mbd2*-knockout mice following intraperitoneal injection of tamoxifen for 5 consecutive days. **(B)** Representative results for coimmunostaining of Coll I and Mbd2 in lung sections from *Mbd2*-C and *Mbd2*-CFKO mice. Nuclei were stained blue by DAPI, and the images were taken at an original magnification of ×400. **(C)** Histological analysis of the severity of lung fibrosis in mice after BLM induction. Left panel: representative images for H&E (top) and Masson staining (bottom). Right panel: A bar graph shows the quantitative mean score of the severity of fibrosis. **(D)** Quantification of hydroxyproline contents in *Mbd2*-CFKO and *Mbd2*-C mice after BLM challenge. **(E)** Western blot analysis of levels of fibronectin, collagen I and α-SMA. **(F-H)** Results for

RT-PCR analysis of *Fn1* **(F)**, *Col1a1* **(G)** and *Acta2* **(H).** Five to six mice were included in each study group. BLM, bleomycin; Fib, Fibronectin; Col I, collagen I; α-SMA, alpha-smooth muscle actin. The data are represented as the mean ± SD. *, $p < 0.05$; **, $p < 0.01$.
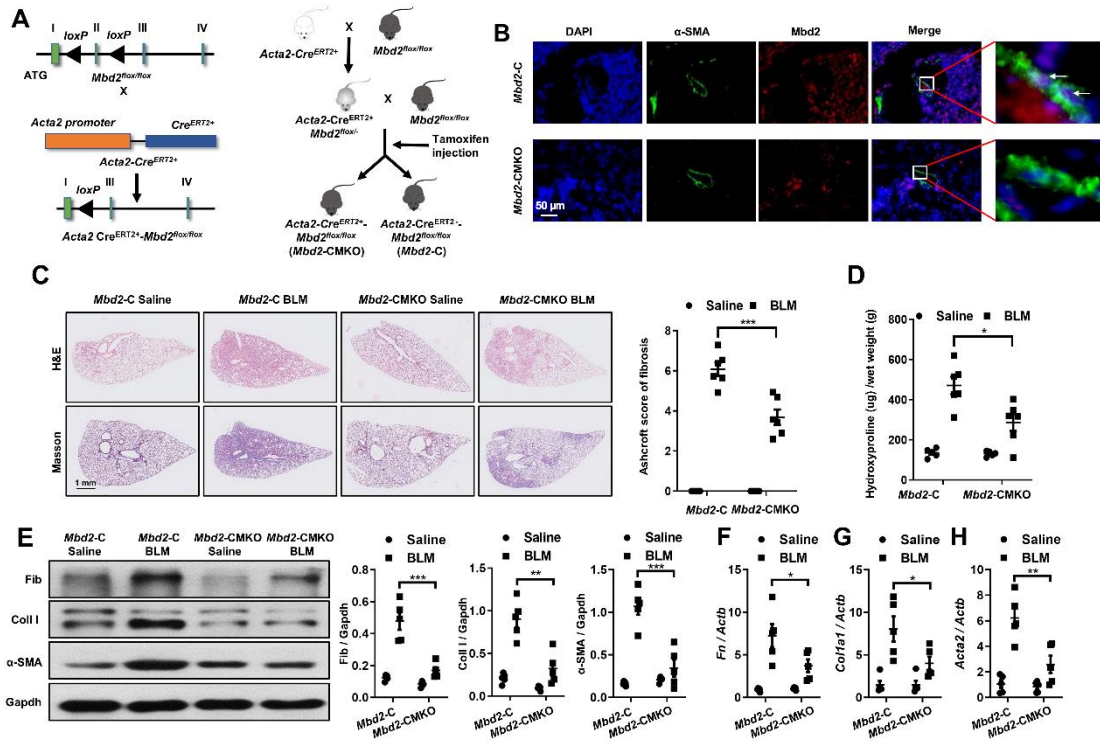
Fig. 5 Comparison of the severity of lung fibrosis between *Mbd2*-CMKO and *Mbd2*-C mice after BLM induction. (A) Schematic illustration of the generation of myofibroblast specific *Mbd2* knockout mice. **(B)** Representative results for coimmunostaining of α-SMA and Mbd2 in lung sections derived from *Mbd2*-C and *Mbd2*-CMKO mice. Nuclei were stained blue by DAPI, and the images were taken at an original magnification of ×400. **(C)** Histological analysis of the severity of lung fibrosis in mice after BLM induction. Left panel: representative images for H&E (top) and Masson staining (bottom). Right panel: A bar graph shows the Ashcroft scores. **(D)** Quantification of hydroxyproline contents in *Mbd2*-CMKO and *Mbd2*-C mice after BLM challenge. **(E)** Western blot analysis of levels of fibronectin, collagen I and α-SMA. **(F-H)** Results for RT-PCR analysis of *Fn1* **(F)**, *Col1a1* **(G)** and *Acta2* **(H).** Five to six mice were included in each study group. BLM, bleomycin; Fib, Fibronectin; Col I, collagen I; α-SMA, alpha-smooth muscle actin. The data are represented as the mean ± SD. *, *p* < 0.05; **, *p* < 0.01, ***, *p* < 0.001.
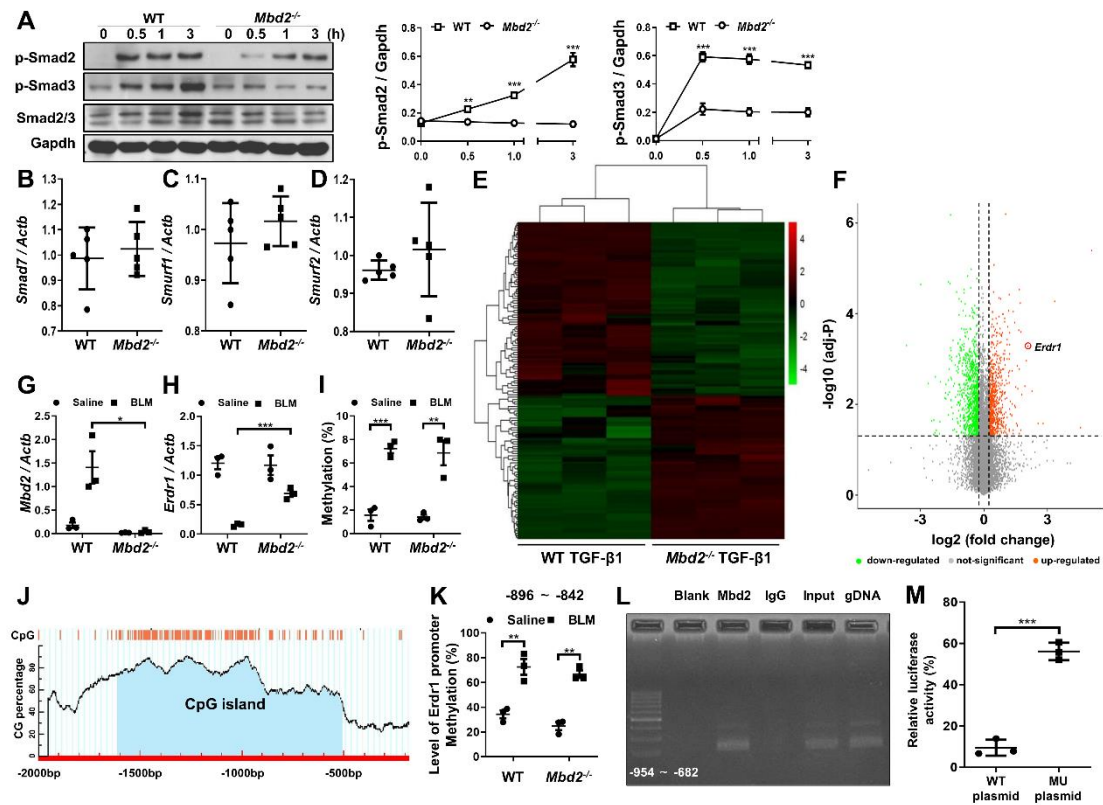
Fig. 6 Mbd2 represses the expression of Erdr1 in fibroblasts following TGF-β1 treatment. (A) Results for time-course Western blot analysis of p-Smad2, p-Smad3 and Smad2/3 expression in fibroblasts following TGF-β1 stimulation. Left panel: Representative Western blot result for p-Smad2, p-Smad3 and Smad2/3 expression at different time points after TGF-β1 stimulation. Right panel: A bar graph shows the results for three replicates. **(B-D)** RT-PCR results for analysis of *Smad7* **(B)**, *Smurf1* **(C)** and *Smurf2* **(D)** expression in lung fibroblasts originated from WT and *Mbd2*^{−/−} mice following TGF-β1 stimulation. **(E-F)** A heat map **(E)** and volcano plot **(F)** for the differentially expressed genes identified by RNA-seq analysis. The color of the heat map represents the fold enrichment in each sample. **(G-H)** RT-PCR analysis of *Mbd2* **(G)** and *Erdr1* **(H)** expression in lung fibroblasts from WT and Mbd2^{−/−} following TGF-β1 stimulation. **(I)** Global DNA methylation rate in fibroblasts after TGF-β1 treatment. **(J)** Predicted CpG island of *Erdr1* promoter. **(K)** Results for the bisulfite DNA sequencing analysis of the *Erdr1* promoter. **(L)** ChIP results for analysis of Mbd2 binding activity to the *Erdr1* promoter. **(M)** Relative luciferase activity in fibroblasts

following TGF-β1 induction. Smurf1, SMAD specific E3 ubiquitin protein ligase 1; Smurf2, SMAD specific E3 ubiquitin protein ligase 2; Erdr1, Erythroid differentiation regulator 1; ChIP, Chromatin Immunoprecipitation. The data are represented as the mean ± SEM of three independent experiments. *, $p < 0.05$; **, $p < 0.01$; ***, $p < 0.001$.
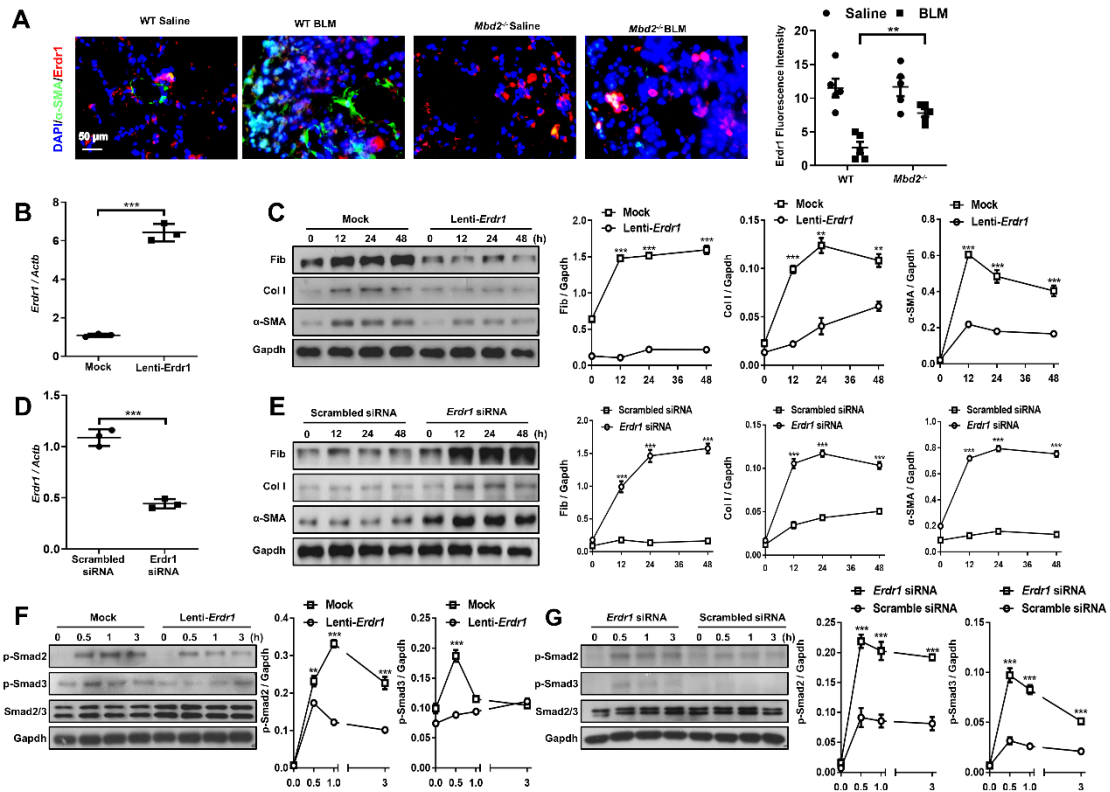
Fig.7 Erdr1 is necessary and sufficient for inhibiting fibroblasts differentiation.
(A) Results for co-immunostaining of Erdr1 and α-SMA in lung sections originated from
WT and *Mbd2^-/-* mice. (B) RT-PCR analysis of *Erdr1* expression in WT fibroblasts
following *Erdr1* lentiviral transduction. (C) Results for time-course Western blot
analysis of fibronectin, collagen I and α-SMA expression in TGF-β1-induced WT
fibroblasts following mock *or Erdr1* lentiviral transduction. Left panel: A representative
Western blot result. Right panel: A bar graph shows the results with three replications.
(D) RT-PCR results for analysis of *Erdr1* expression in TGF-β1-induced *Mbd2^-/-*
fibroblasts transfected with an *Erdr1* siRNA. (E) Results for a time-course Western blot
analysis of fibronectin, collagen I and α-SMA expression in TGF-β1-induced *Mbd2^-/-*
fibroblasts transfected with *a* scrambled or an *Erdr1* siRNA. Left panel: A
representative Western blot result. Right panel: A bar graph shows the results with
three replications. (F) Results for time-course Western blot analysis of p-Smad2 and
p-Smad3 levels in mock or *Erdr1* lentiviral transduced WT fibroblasts following TGF-
β1 stimulation. (G) A time-course Western blot analysis of p-Smad2 and p-Smad3

levels in scrambled or *Erdr1* siRNA transfected *Mbd2*$^{-/-}$ fibroblasts following TGF-β1 stimulation. BLM, bleomycin; Fib, Fibronectin; Col I, collagen I; α-SMA, alpha-smooth muscle actin; Erdr1, Erythroid differentiation regulator 1. The data are represented as the mean ± SEM of three independent experiments. **, $p < 0.01$; ***, $p < 0.001$.
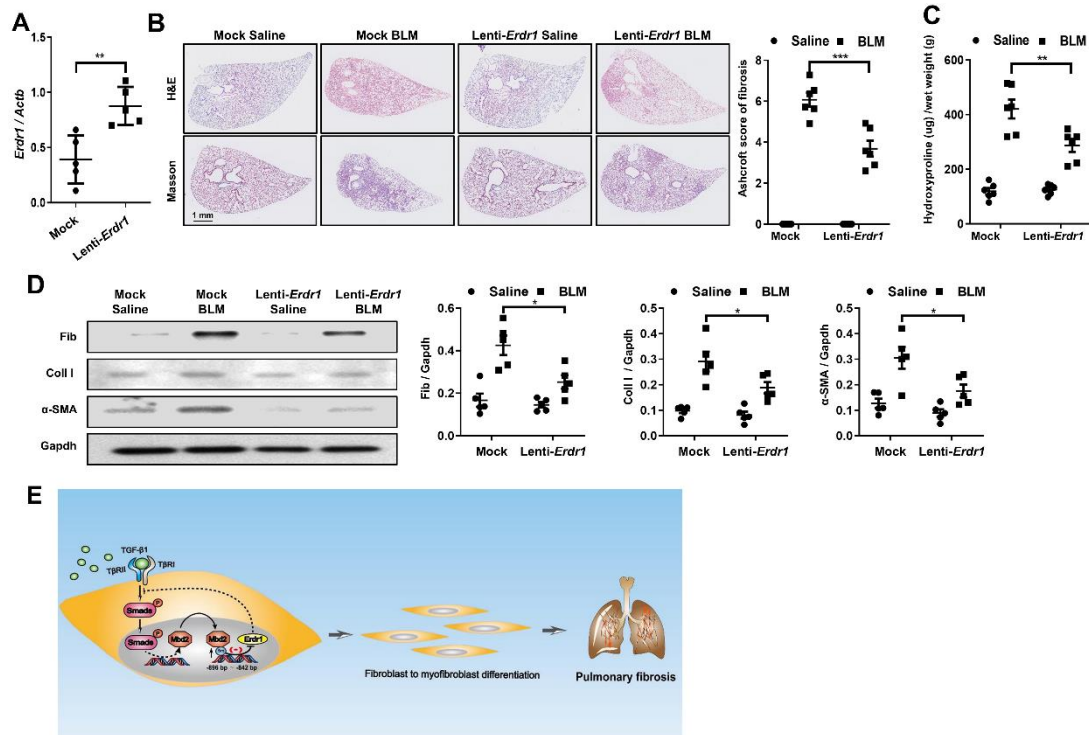
**Fig. 8 Ectopic Erdr1 expression protected mice from BLM-induced lung fibrosis.**
(A) RT-PCR analysis of *Erdr1* expression in BLM-induced lungs following *Erdr1* lentiviral transduction. **(B)** Lentiviral delivered *Erdr1* expression protected mice from BLM-induced pulmonary fibrosis. Left panel: Representative results for H&E and Masson staining, Right panel: The semiquantitative Ashcroft scores relevant to the severity of fibrosis. **(C)** Quantification of hydroxyproline contents in mice transduced with lentiviruses after BLM challenge. **(D)** Western blot for analysis of fibronectin, collagen I and α-SMA expression. **(E)** A diagram for mechanisms underlying MBD2 regulation of fibroblast differentiation, in which TGF-β induces Mbd2 overexpression in a TβRI/Smad3-dependent manner, and then, Mbd2 selectively bound to the regions of *Erdr1* promoter to repress its expression, through which it enhanced TGF-β/Smads signaling to promote fibroblast differentiating into myofibroblast. Five to six mice were included in each study group. BLM, bleomycin; Fib, Fibronectin; Col I, collagen I; α-SMA, alpha-smooth muscle actin. The data are represented as the mean ± SD. *, $p < 0.05$; **, $p < 0.01$, ***, $p < 0.001$.
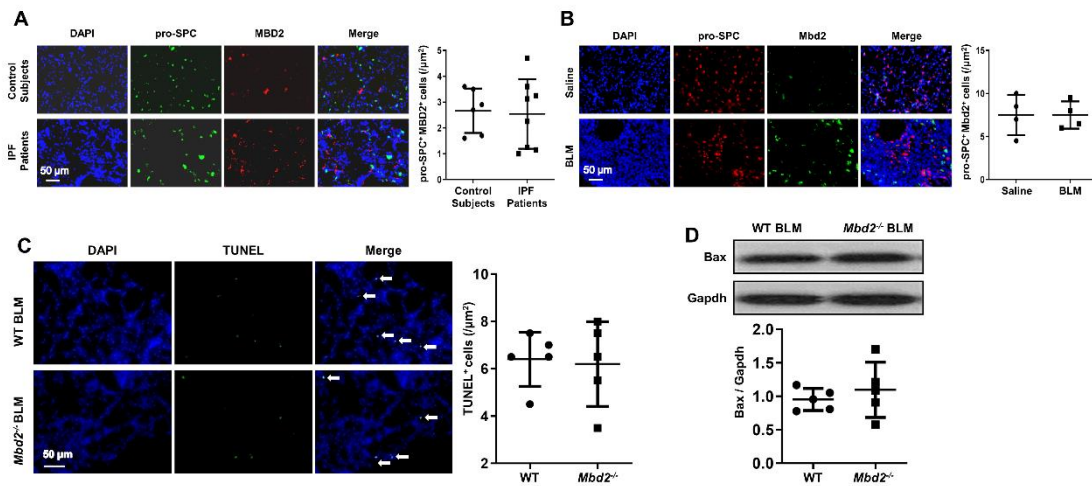
Supplementary Fig. 1 (A-B) Representative results for coimmunostaining of MBD2 and pro-SPC, a marker of AECII in the lung sections from patients with control subjects and IPF patients **(A)** and BLM-induced lung sections **(B)**. The nuclei were stained blue by DAPI, and the images were taken under original magnification ×400. **(C)** Representative results for TUNEL assays of lung sections originated from BLM-induced WT and *Mbd2*^-/- mice. Nuclei were stained with DAPI (blue), and images were captured at ×200 magnification. **(D)** Western blot analysis of Bax expression in lungs originated from WT and *Mbd2*^-/- mice following BLM induced. pro-SPC: Prosurfactant Protein C. Four to five mice were included in each study group.
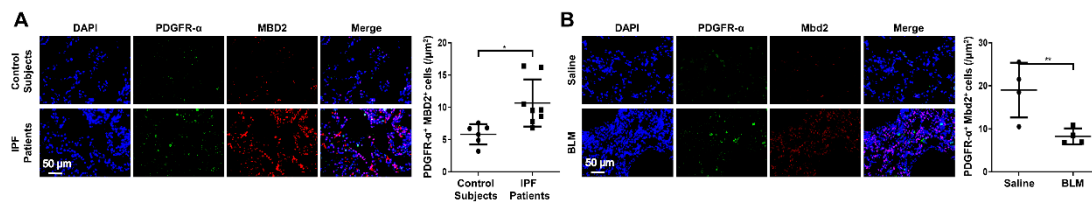
Supplementary Fig. 2 (A-B) Representative results for coimmunostaining of MBD2 and PDGFR-α in the lung sections from patients with control subjects and IPF patients **(A)** and BLM-induced lung sections **(B)**. The nuclei were stained blue by DAPI, and the images were taken under original magnification ×400. A total of eight patients with IPF and six control subjects were analyzed. Four mice were included in each study group. The data are represented as the mean ± SD. *, $p < 0.05$; **, $p < 0.01$.
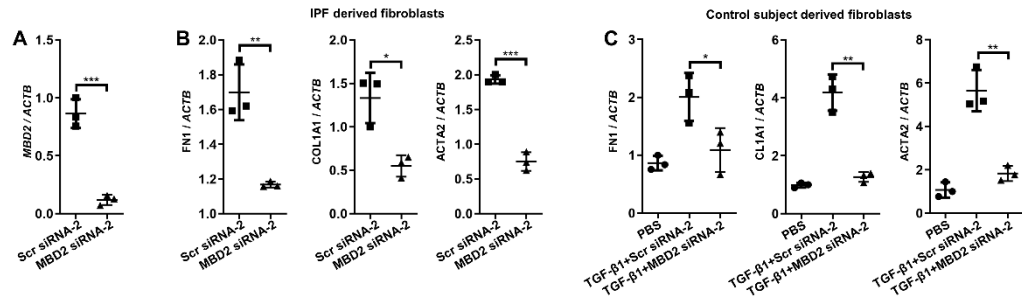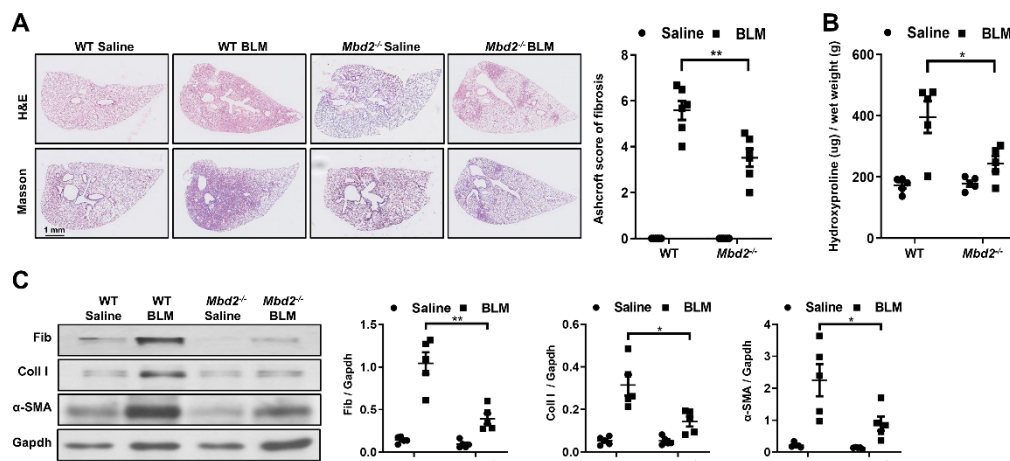
Supplementary Fig. 3 (A) RT-PCR analysis of the *MBD2* expression after *MBD2* siRNA-2 transinfected. **(B-C)** RT-PCR analysis of the expression of FN1, COL1A1 and ACTA2 in IPF patient **(B)** and control subject's **(C)** lung derived fibroblasts. The data are represented as the mean ± SEM of three independent experiments. *, $p < 0.05$; **, $p < 0.01$; ***, $p < 0.001$.
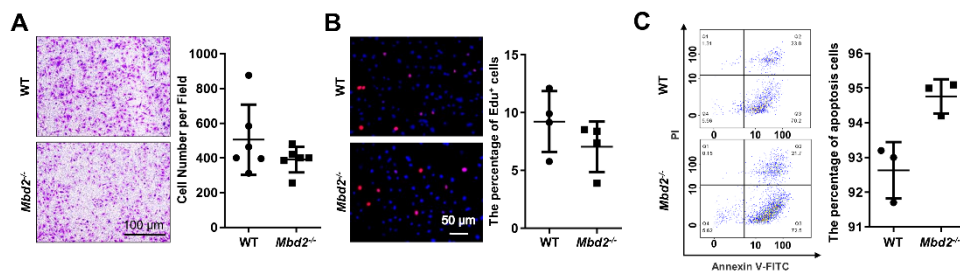
Supplementary Fig. 4 (A) Transwell assay analysis of WT and *Mbd2*$^{-/-}$ fibroblast migration. **(B)** EdU staining analysis of WT and *Mbd2*$^{-/-}$ fibroblast proliferation. The nuclei were stained blue by DAPI, and the images were taken under original magnification ×200. **(C)** Annexin V/PI staining analysis of WT and *Mbd2*$^{-/-}$ fibroblast apoptosis. The data are represented as the mean ± SEM of three independent experiments.
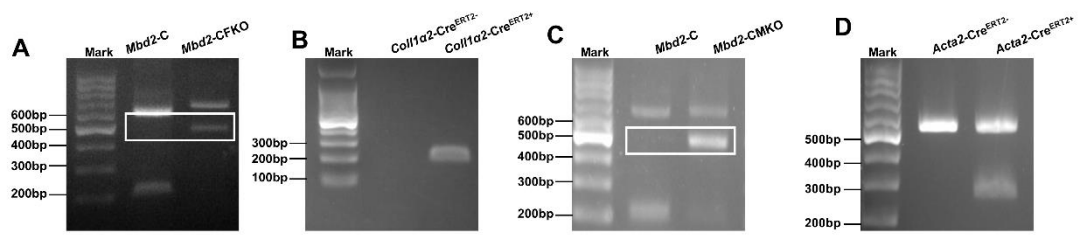
Supplementary Fig. 5 (A-B) Genotyping results of *Coll1a2*-Cre^{ERT2+}*Mbd2*$^{flox/flox}$ allele.

(C-D) Genotyping results of *Acta2*-Cre^{ERT2+}*Mbd2*$^{flox/flox}$ allele.

Supplementary Fig. 6 (A) Histological analysis of the severity of lung fibrosis in mice after BLM induction. Left panel, representative images for H&E (top) and Masson staining (bottom). Right panel: A bar graph shows the quantitative mean score of the severity of fibrosis. **(B)** Quantification of hydroxyproline contents in WT and *Mbd2* mice after BLM challenge. **(C)** Western blot analysis of levels of fibronectin, collagen I and α-SMA. Left panel: A representative Western blot result. Right panel: A bar graph shows the mean data from all mice analyzed in each group. Five to six mice were included in each study group. BLM, bleomycin; Fib, Fibronectin; Col I, collagen I; α-SMA, alpha-smooth muscle actin. Five to six mice were included in each study group. *, $p < 0.05$; **, $p < 0.01$.
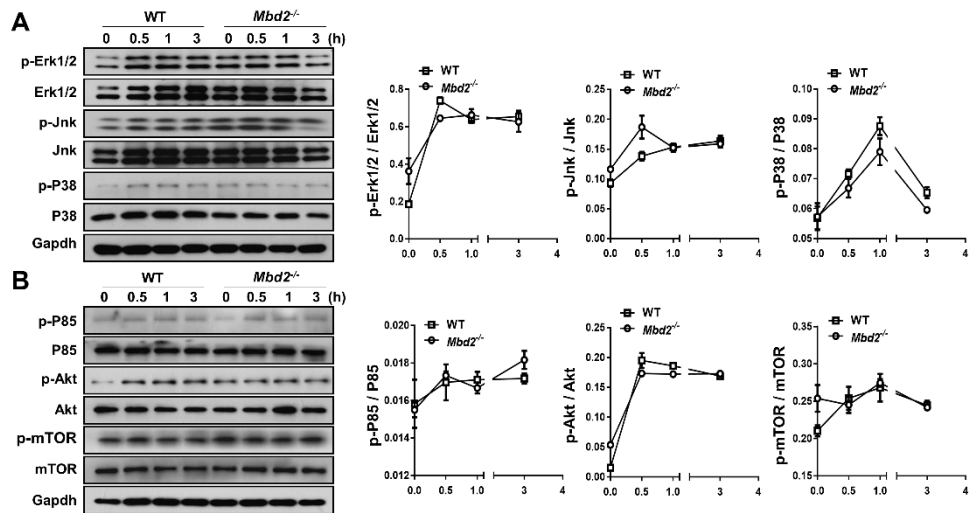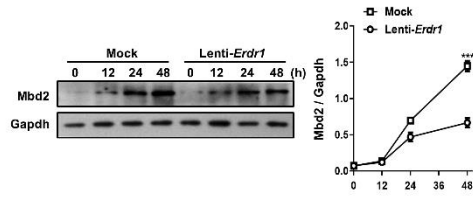
Supplementary Fig. 7 (A) A time-course analysis of the Levels of Erk1/2, p-Erk1/2, Jnk, p-Jnk, P38 and p-P38 in fibroblasts following TGF-β1 treatment. **(B)** A time-course Western blot analysis of P85, p-P85, Akt, p-AKT, mTOR and p-mTOR expression in fibroblasts following TGF-β1 stimulation.
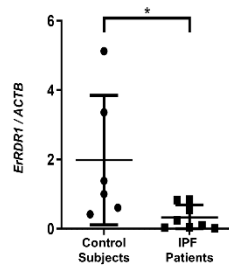
Supplementary Fig. 8 Results for RT-PCR analysis of *ERDR1* expression in lung tissues from IPF patients and control subjects. *, *p* < 0.05.
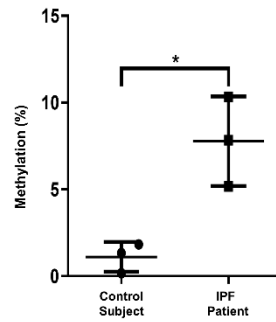
Supplementary Fig. 9 Global DNA methylation rate in fibroblasts from IPF patient and control subject's lung. *, $p < 0.05$.

Supplementary Fig. 10 Results for time-course Western blot analysis of Mbd2 expression in TGF-β1-induced WT fibroblasts following mock *or Erdr1* lentiviral transduction. Left panel: A representative Western blot result. Right panel: A bar graph shows the results with three replications. ***, $p < 0.001$.

Supplementary Table 1. Characteristics of subjects for lung samples

	Lung samples		P value
	IPF　(N = 8)	Control　(N = 6)	
Age (years)	58.50 ± 3.645	55.17 ± 6.024	0.6265
Smoking index	41.10 ± 19.15	46.58 ±24.90	0.8620
BMI	22.18 ± 1.170	23.40 ± 0.3360	0.3966
Sex 　Female 　Male	 3 (37.50%) 5 (62.50%)	 2 (33.33%) 4(66.67%)	0.8860
FVC Percent Predicted	65.04 ± 4.565	NA	
DLCO	42.10 ± 4.011	NA	

FVC: Forced vital capacity　　　DLCO: diffusion capacity for carbon monoxide

Supplementary Table 2. The primer sequences for RT-PCR

human *FN1*	forward	5′-GAT GTC CGA ACA GCT ATT TAC CA-3′
	reverse	5′-CGA CCA CAT AGG AAG TCC CAG-3′
human *COL1A1*	forward	5′-GAG GGC CAA GAC GAA GAC ATC-3′
	reverse	5′-CAG ATC ACG TCA TCG CAC AAC-3′
human *ACTA2*	forward	5′-GAC GCT GAA GTA TCC GAT AGA ACA CG-3′
	reverse	5′-CAC CAT CTC CAG AGT CCA GCA CAA T-3′
human *ACTB*	forward	5′-AGC GAG CAT CCC CCA AAG TT-3′
	reverse	5′-GGG CAC GAA GGC TCA TCA TT-3′
mouse *Fn1*	forward	5′-ATG CAA CGA TCA GGA CAC AA -3′
	reverse	5′-TGT GCC TCT CAC ACT TCC AC-3′
mouse *Col1a1*	forward	5′-CCT GGT AAA GAT GGT GCC-3′
	reverse	5′-CAC CAG GTT CAC CTT TCG CAC C-3′
mouse *Acta2*	forward	5′-CGT ACA ACT GGT ATT GTG CTG GAC-3′
	reverse	5′-TGA TGT CAC GGA CAA TCT CAC GCT-3′
mouse *Actb*	forward	5′-TGA CGT TGA CAT CCG TAA AGA CC-3′
	reverse	5′-CTC AGG AGG AGC AAT GAT CTT GA-3′